Inorganic Chemistry

pubs.acs.org/IC
Article

Structural and Magnetic Studies of ABO_4-Type Ruthenium and Osmium Oxides

Sean Injac, Alexander K. L. Yuen, Maxim Avdeev, Chun-Hai Wang, Peter Turner, Helen E. A. Brand, and Brendan J. Kennedy*

Cite This: https://dx.doi.org/10.1021/acs.inorgchem.9b03118

ABSTRACT: Oxides of the form ABO_4 with A = K, Rb, Cs and B = Ru and Os have been synthesized and characterized by diffraction and magnetic techniques. For A = K the oxides adopted the tetragonal ($I4_1/a$) scheelite structure. $RbOsO_4$, which crystallizes as a scheelite at room temperature, underwent a continuous phase transition to $I4_1/amd$ near 550 K. $RbRuO_4$ and $CsOsO_4$ were found to crystallize in the orthorhombic ($Pnma$) pseudoscheelite structure, and both displayed discontinuous phase transitions to $I4_1/a$ at high temperatures. $CsOsO_4$ was determined to undergo a phase transition to a $P2_1/c$ structure below 140 K. $CsRuO_4$ crystallizes with a baryte-type structure at room temperature. Upon heating $CsRuO_4$ a first order phase transition to the scheelite structure in $I4_1/a$ is observed at 400 K. A continuous phase transition is observed to $P2_12_12_1$ below 140 K. DC magnetic susceptibility data is consistent with long-range antiferromagnetic ordering at low temperatures for all compounds except for $CsOsO_4$, which is paramagnetic to 2 K. The effective magnetic moments are in agreement with the spin only values for an $S = 1/2$ quantum magnet. Effective magnetic moments calculated for Os compounds were lower than their Ru counterparts, reflective of an enhanced spin orbit coupling effect. A magnetic structure is proposed for $RbRuO_4$ consisting of predominately antiferromagnetic (AFM) ordering along the 001 direction, with canting of spins in the 100 plane. A small ordered magnetic moment of 0.77 μ_B was determined.

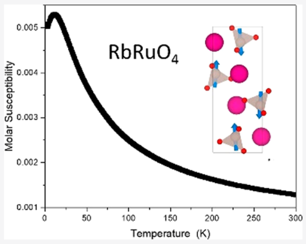

INTRODUCTION

Transition metals are vital in many technologically important materials. In particular, the complex interplay between the spin, lattice, and orbital degrees of freedom can result in the emergence of unique properties including superconductivity, colossal magnetoresistance, and magnetism. Recent focus on 4d and 5d transition metal oxides has revealed a delicate balance between the spin−orbit interactions and the crystalline electric field that play a critical role in the generation of novel magnetic states. The spatial extension of the d orbitals and the spin−orbit coupling are both considerably larger in the 5d system than in their 4d analogues.

The majority of magnetic 4d and 5d systems described to date has the transition metal in an octahedral, or distorted variant thereof, crystal field. Recently the possibility of using tetrahedral crystal fields to generate new magnetic materials incorporating 4d and 5d transition metals has emerged as an exciting field of research.[1] In general, tetrahedral coordination results in a high spin ground state in oxides, although Zhou et al. recently reported the formation of the low spin Ir^V $e^4t_2^0$ state with tetrahedral coordination in $Sr_9Ir_3O_{17}$.[2]

The ABO_4 tetragonal scheelite ($CaWO_4$) structure contains a large low valent A-type cation and a smaller high valent B-type cation. The B-type cation is bonded to four oxygen atoms in a distorted tetrahedra. The BO_4 tetrahedra are isolated from each other by AO_8 polyhedra. Early structural studies of $AReO_4$ perrhenates by Rogner and Range established that it was possible to stabilize an alternate orthorhombic structure that contains the same BO_4 topology by increasing the size of the A-type cation.[3−6] Since these perrhenates contain the 5d^0 Re^{VII} cation, they are diamagnetic. Similar, but not identical, structures have been reported for the corresponding diamagnetic pertechnetates that contain the 4d^0 Tc^{VII} cation.[7,8]

Silverman described $KRuO_4$ (Ru^{VII} 4d^1) as having the tetragonal scheelite structure but did not report its magnetic properties.[9] Marjerrison and co-workers, using powder neutron diffraction, confirmed the structure of $KRuO_4$ and, from bulk magnetic susceptibility measurements, showed this has an effective magnetic moment of 1.73 μ_B with a large Weiss constant of −76 K indicative of antiferromagnetism.[10] The ordered magnetic structure was established to have k = (000) with a small ordered moment for the Ru^{VII} of 0.57(7) μ_B. Leevason[11] reported that $KOsO_4$ is isostructural with $KRuO_4$ and stated that μ_{eff} at 298 K was 1.4 μ_B which is consistent with a 5d^1 configuration of Os^{VII}.

Shortly after the work of Marjerrison on $KRuO_4$ was published, Yamaura and Hiroi and Injac and co-workers

Received: October 28, 2019

Table 1. Summary of Structures of the ABO_4 Oxides (A = K, Rb, Cs; B = Ru, Os)[a]

composition	$KRuO_4$	$RbRuO_4$	$RbRuO_4$	$CsRuO_4$	$CsRuO_4$	$CsRuO_4$
temperature (K)	298	298	500	90	298	500
space group	$I4_1/a$	$Pnma$	$I4_1/a$	$P2_12_12_1$	$Pnma$	$I4_1/a$
a (Å)	5.60961(2)	5.50821(7)	5.71893(6)	7.18415(6)	8.40128(1)	5.88079(3)
b (Å)	5.60961(2)	5.75022(7)	5.71893(6)	7.85517(5)	7.17776(1)	5.88079(3)
c (Å)	12.96261(4)	13.7683(2)	13.93628(3)	8.19231(6)	8.04343(1)	14.59233(7)
volume (Å^3)	407.903(2)	436.090(9)	455.803(2)	462.3136(12)	485.037(9)	504.6573(8)
A x	0	0.0267(6)	0	0.2178(1)	0.6297(1)	0
A y	0.25	0.25	0.25	0.4091(2)	0.25	0.25
A z	0.625	0.125	0.625	0.3707(1)	0.1468(1)	0.625
A B_{iso} (Å^2)	2.19(4)	2.06(6)	5.16(7)	0.809(9)	2.76(3)	5.219(5)
Ru x	0	0.9619(6)	0	0.2562(1)	0.8789(2)	0
Ru y	0.25	0.25	0.25	0.9132(2)	0.75	0.25
Ru z	0.125	0.9179(3)	0.125	0.3770(2)	0.1531(2)	0.125
Ru B_{iso} (Å^2)	0.72(2)	2.14(6)	2.94(6)	0.184(1)	1.058(3)	3.224(1)
O_1 x	0.1073(3)	0.1639(9)	0.9303(8)	0.0632(1)	0.3813(9)	0.9742(8)
O_1 y	0.0198(3)	0.25	0.4936(5)	0.0364(1)	0.9417(4)	0.0257(6)
O_1 z	0.1976(2)	0.62225(2)	0.1701(2)	0.3976(2)	0.2215(4)	0.1845(5)
O_1 B_{iso} (Å^2)	2.51(4)	2.87(9)	7.57(8)	2.71(9)	2.97(9)	7.99(9)
O_2 x		0.6428(7)		0.4392(1)	0.4565(8)	
O_2 y		0.25		0.0417(1)	0.25	
O_2 z		0.9801(4)		0.3427(2)	0.5142(7)	
O_2 B_{iso} (Å^2)		3.91(12)		2.71(9)	5.00(24)	
O_3 x		0.9806(8)		0.2849(2)	0.7945(7)	
O_3 y		0.9945(6)		0.7819(1)	0.25	
O_3 z		0.3128(2)		0.5414(1)	0.5395(8)	
O_3 B_{iso} (Å^2)		3.53(8)		2.71(9)	5.14(22)	
O_4 x				0.2052(1)		
O_4 y				0.8087(1)		
O_4 z				0.2076(3)		
O_4 B_{iso} (Å^2)				2.71(9)		
Ru−O_1 (Å)	1.708(2) × 4	1.744(6)	1.579(8) × 4	1.734(1)	1.706(3)	1.587(1) × 4
Ru−O_2 (Å)		1.757(5)		1.730(1)	1.762(6)	
Ru−O_3 (Å)		1.676(3) × 2		1.728(1)	1.720(6) × 2	
Ru−O_4 (Å)				1.729(1)		
Ru−Ru (Å)	4.286(1)	4.408(1), 4.505(3)	4.520(3)	4.327(1), 4.855(1)	4.481(1), 4.804(2)	4.679(1)
A BVS	1.23	1.07			0.62	
Ru BVS	8.58	8.49			8.23	
χ^2 SXRD, NPD	1.94, 2.75	1.21, 3.02	1.63	2.66	3.26, 2.48	1.86
R_{Bragg} (SXRD, NPD)	3.06, 4.03	2.83, 2.73	6.31	4.59	3.02, 3.33	4.80
R_{WP} (SXRD, NPD)	3.56, 4.98	3.35, 3.48	7.29	6.27	3.86, 4.17	5.88
composition	$KOsO_4$	$RbOsO_4$	$RbOsO_4$	$CsOsO_4$	$CsOsO_4$	$CsOsO_4$
temperature (K)	298	298	573	90	298	470
space group	$I4_1/a$	$I4_1/a$	$I4_1/amd$	$P2_1/c$	$Pnma$	$I4_1/a$
a (Å)	5.67586(1)	5.81846(1)	5.80443(2)	8.22278(11)	5.75848(1)	5.92808(9)
b (Å)	5.67586(1)	5.81846(1)	5.80443(2)	7.921734(7)	5.93846(1)	5.92808(9)
c (Å)	12.71914(1)	13.34350(2)	13.8860(5)	8.23025(11)	14.35759(9)	14.46877(3)
β (deg)				119.0845(6)		
volume (Å^3)	409.7531(17)	451.737(4)	467.841(17)	468.506(15)	490.984(4)	508.466(13)
A x	0	0	0	0.2366(14)	0.9744(9)	0
A y	0.25	0.25	0.75	0.1098(4)	0.25	0.25
A z	0.625	0.625	0.125	0.9928(4)	0.6249(5)	0.625
A B_{iso} (Å^2)	1.85(5)	2.26(14)	7.64(10)	0.89(12)	2.94(13)	5.05(15)
Os x	0	0	0	0.7581(2)	0.0354(6)	0
Os y	0.25	0.25	0.25	0.4173(4)	0.25	0.25
Os z	0.125	0.125	0.375	0.8709(3)	0.1213(3)	0.125
Os B_{iso} (Å^2)	1.41(1)	1.46(5)	6.72(6)	3.85(14)	2.76(9)	4.37(9)
O_1 x	0.1196(4)	0.9280(43)	0	0.6258	0.3162(27)	0.0173(30)
O_1 y	0.0214(4)	0.4609(33)	0.4782*	0.9531	0.25	0.019(9)
O_1 z	0.1978(2)	0.2080(16)	0.6966*	0.3158	0.0833(9)	0.1877(4)
O_1 B_{iso} (Å^2)	2.59(4)	3.48(9)	17.36(62)	1.00*	4.15(13)	7.56(29)

https://dx.doi.org/10.1021/acs.inorgchem.9b03118
Inorg. Chem. XXXX, XXX, XXX−XXX

Table 1. continued

composition	$KOsO_4$	$RbOsO_4$	$RbOsO_4$	$CsOsO_4$	$CsOsO_4$	$CsOsO_4$
O_2 x				0.8386	0.3473(27)	
O_2 y				0.9688	0.25	
O_2 z				0.7031	0.4688(13)	
O_2 B_{iso} ($Å^2$)				1.00*	8.60(24)	
O_3 x				0.9244	0.5064(21)	
O_3 y				0.1877	0.5128(13)	
O_3 z				0.4652	0.6869(5)	
O_3 B_{iso} ($Å^2$)				1.00*	4.17(23)	
O_4 x				0.6205		
O_4 y				0.2511		
O_4 z				0.5252		
O_4 B_{iso} ($Å^2$)				1.00*		
Os–O_1 (Å)	1.732(2) × 4	1.704(20) × 4	1.865 × 4	1.738(9)	1.692(17)	1.699(8) × 4
Os–O_2 (Å)				1.689(10)	1.680(2)	
Os–O_3 (Å)				1.792(14)	1.707(9) × 2	
Os–O_4 (Å)				1.779(11)		
Os–Os (Å)	4.262(1)	4.426(1)	4.525(5)	4.34(3), 4.890(4)	4.689(7), 4.591(7))	4.6784(5)
A BVS	1.28	0.88	1.79	1.14	0.59	1.9
Os BVS	7.2	7.8	4.91	6.89	7.31	7.9
χ^2 SXRD, NPD	2.96, 1.72	2.29, 2.68	1.14	4.53	6.64, 7.05	6.56, 4.84
R_{Bragg} (SXRD, NPD)	3.27, 2.50	9.74, 3.23	4.41	4.98	4.04, 4.49	6.10, 4.66
R_{WP} (SXRD, NPD)	3.79, 3.14	11.0, 4.18	4.58	5.72	6.25, 7.36	10.2, 6.33

[a] The structures at room temperature (298 K) were refined against a combined synchrotron X-ray (S-XRD) and Neutron (NPD) data set. All other structures were refined against S-XRD data alone. Values marked with an (*) were not allowed to vary during the refinement.

independently reported the structure and magnetic susceptibility of $KOsO_4$.[12,13] Both groups reported μ_{eff} of ~1.4 μ_B and $\theta = -44$ K showing the material to be an antiferromagnet. Injac revealed, using powder neutron diffraction, $KOsO_4$ to have the same AFM structure as $KRuO_4$ with the ordered moment of the Os^{VII} being 0.5 μ_B. The experimental studies of Injac verified the earlier results of Song et al.[14] that had prompted theoretical studies of Hayami and co-workers,[15] predicting the emergence of odd parity multipoles associated with spin and orbital ordering in $KOsO_4$.

Given the paucity of oxides where a magnetic 4*d* and 5*d* cation exists in a tetrahedral coordination, we have prepared and characterized other members of the ABO_4 scheelites where B = Ru or Os. Neutron diffraction has been used to obtain accurate and precise structures.

■ EXPERIMENTAL SECTION

Hazards. ***Caution!*** *RuO_4 is an extremely strong oxidizing agent, which will spontaneously combust or explode in the presence of organic solvents.*[16] *Heating above 100 °C results in explosive decomposition. RuO_4 readily sublimes at room temperature. No attempt was made to isolate pure RuO_4. OsO_4 is an extremely toxic, corrosive, and potentially lethal oxidizing agent. The compound is lethal by inhalation, skin contact, and ingestion and will cause blindness if in contact with eyes. Appropriate PPE including sealed goggles and Latex gloves were used for all manipulations where RuO_4 or OsO_4 could be present and always in a fumehood.*

Synthesis. The $ARuO_4$ (A = K, Rb, Cs) perruthenates were synthesized by reduction of a chloroform solution of RuO_4 using an aqueous solution of the appropriate AOH hydroxide. $RuCl_3 \cdot 2H_2O$ was reacted with 4 mol equiv of $NaIO_4$ in a mixture of 50 mL of distilled $CHCl_3$ (free from any ethanol or amylene stabilizer) and 100 mL of H_2O in order to yield 1 g of RuO_4. The mixture was stirred vigorously overnight during which time the aqueous layer turned clear and the chloroform layer became a golden color. The chloroform layer was separated and decanted into a 100 mL flask, using a 0.1 M aqueous solution of the appropriate hydroxide. This mixture was again stirred vigorously overnight at which time the chloroform layer was clear and colorless. The aqueous layer was decanted into an evaporating basin and evaporated at 100 °C until yellow-green crystals were recovered. In the case of $CsRuO_4$, crystals precipitated without reduction of the solvent volume.

The $AOsO_4$ (A = K, Rb, Cs) perosmates were synthesized by reduction of OsO_4 with the appropriate iodide salt of the A-type cation. All manipulations were performed using standard Schlenk techniques. A solution of 1 g of OsO_4 dissolved in approximately 20 mL of dried acetone was transferred, via canula, to a solution containing a 1.5 molar ratio of AI dissolved in a minimum amount of dried acetone. This solution was stirred at room temperature until it turned dark red. The solvent volume was reduced until a black precipitate formed. This precipitate was separated, using a centrifuge, and washed with cold acetone.

Physical Methods. Neutron powder diffraction (NPD) data were measured at room temperature using the high-resolution powder diffractometer Echidna at ANSTO's OPAL reactor, using a wavelength of 1.622 Å.[17] Variable temperatures were achieved using a cryofurnace. Synchrotron X-ray powder diffraction data were collected over the angular range $5 < 2\theta < 85°$, using X-rays of wavelength 0.56154 Å, as determined by structural refinement of a diluted NIST SRM660b LaB_6 standard, on the powder diffractometer at beamline BL-10 of the Australian Synchrotron.[18] Temperatures were achieved using a Cyberstar hot-air blower and were increased at a rate of 5 °C/min data. Temperatures were calibrated using a combination of thermocouple measurements and a range of melting-point and phase-transition standards. The samples were housed in 0.2 mm diameter quartz capillaries that were rotated during the measurements.

Structure refinements, using the Rietveld method, were undertaken using the FullProf software suite with the WinPlotr interface.[19,20] The peak shapes were modeled using a Thompson-Cox-Hastings pseudo-Voigt with axial divergence asymmetry profile function, and the background was modeled using linear interpolation between points with refinable intensities. The scale factor, detector zero-point, lattice parameters, atomic coordinates, and atomic displacement parameters were refined together with the peak profile parameters.

Single crystal diffraction data were measured using a Rigaku Oxford Diffraction SuperNova Dual diffractometer equipped with an Atlas CCD detector and employing mirror monochromated Mo–Kα or

Cu−Kα radiation generated from a microsource used for data collection. The structures were solved by direct methods. Further details are provided in the SI.

Magnetic susceptibilities were measured using a Quantum Design Physical Properties Measurement System (PPMS). Temperature-dependent DC magnetic susceptibility measurements were taken under zero field-cooled (ZFC) upon heating, and field-cooled (FC) upon cooling conditions over the range 2−300 K, in an applied field of 0.1 T. Isothermal field-dependent magnetization data were collected to ±9 T at constant temperatures. Heat capacity measurements were undertaken on pressed pellets using the same PPMS platform. Variable temperature heat capacity data were analyzed by modeling the lattice contribution to heat capacity using a fifth order polynomial fit, which was subtracted from the total heat capacity about the magnetic anomaly. In the case of $KRuO_4$ and $KOsO_4$, the lattice contribution to heat capacity was subtracted by the heat capacity of the isostructural and diamagnetic $KReO_4$. Values of ΔS_{mag} were effectively equivalent using either technique to model the lattice contribution.

■ RESULTS AND DISCUSSION

1. Room Temperature Structures. The three oxides, $KOsO_4$, $RbOsO_4$, and $KRuO_4$, display a tetragonal scheelite-type structure described in space group $I4_1/a$ at room temperature. In scheelite the *A*- and *B*-type cations are at the 4*a* (0 1/4 1/8) and 4*b* (0 1/4 1/8) special positions, respectively. The results of the Rietveld refinements against the neutron and synchrotron diffraction data are summarized in Table 1, representative Rietveld plots are shown in Figure 1, and others are available in the SI Figures S1−S3. The oxygen occupies the 16*f* general position with $x \sim 1/8$, $y \sim 0$, and $z \sim 1/4$. In this structure there is a single *B*−O distance of 1.732(2), 1.704(20), and 1.708(2) Å for $KOsO_4$, $RbOsO_4$, and $KRuO_4$, respectively. The latter value is in reasonable agreement with that reported by Marjerrison et al.[10] for $KRuO_4$ at 280 K of 1.742(4) Å and is approximately equal to the sum of the ionic radii of four-coordinate Ru^{VII} (0.38 Å) and three-coordinate O^{2-} (1.36 Å) reported by Shannon.[21] Shannon does not list an ionic radius for four-coordinate Os^{VII}, but the present results suggest a value of about 0.38 Å would be appropriate. We will return to this shortly. That the ionic radius of the 5*d* Os^{VII} cation is approximately equal to that of the 4*d* Ru^{VII} cation is a consequence of the occupancy of the intervening 4*f* levels, the lanthanide contraction. The remaining three oxides, $RbRuO_4$, $CsOsO_4$, and $CsRuO_4$, are all orthorhombic in space group *Pnma*. However, they are not isostructural. $RbRuO_4$ and $CsOsO_4$ have the pseudoscheelite structure that has been described for the corresponding Re and Tc oxides, $CsReO_4$ and $CsTcO_4$.[7,8] The formation of the pseudoscheelite structure is favored as the ratio of the ionic radii r_A/r_B increases.[3,5,6] The average Os−O distance in $CsOsO_4$ is 1.697 Å and is similar to that seen for $KOsO_4$ and $RbOsO_4$. Likewise, the Ru−O distance of 1.713 Å in $RbRuO_4$ is similar to that of $KRuO_4$.

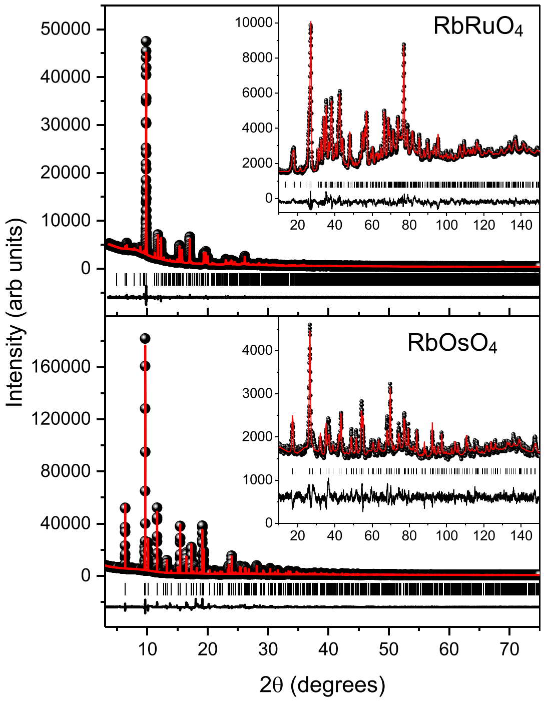

Figure 1. Examples of the S-XRD and NPD Rietveld fits for $RbRuO_4$ and $RbOsO_4$, with data collected at room temperature. In this figure the insets are the NPD profiles. Black circles represent the collected data, the red line indicates the fit, and black vertical marks indicate the locations of allowed reflections.

We have recently demonstrated for the analogous $AReO_4$ oxides that in tetragonal scheelite-type structures the distortion of the BO_4 tetrahedra correlates with the size of the *A*-type cation with the bond angles moving away from the ideal value of 109° as the size of the *A*-cation increases.[22] This trend is followed for the pair of oxides $KOsO_4$ and $RbOsO_4$.

The unit cell parameters ($a = 8.40128(1)$, $b = 7.17776(1)$, $c = 8.04343(1)$ Å) of $CsRuO_4$ are distinctly different than those of scheelite $a \sim 5.9$, $c \sim 14.6$ Å. These parameters are similar to that of baryte ($BaSO_4$) although the *b*-axis is noticeably longer. The structure is practically equivalent to that reported for $PbSO_4$ anglesite by Santamaria-Perez et al.[23] Since the synthesis of $CsRuO_4$ produced small, diffraction-quality single crystals, the structure was solved using single crystal methods. In $CsRuO_4$, as in baryte, the two cations are on a mirror plane; however, the three oxygen atoms all occupy 8*d* general positions. Like scheelite, the $CsRuO_4$ structure contains isolated RuO_4 tetrahedra. The average Ru−O distance is 1.727 Å. The cesium cation is coordinated by a total of nine oxygen atoms with distances between 3.036 and 3.294 Å and has three longer Cs−O bonds, one at 3.449 and two at 3.746 Å. This arrangement is different than that of the Ba cation in baryte which is 12-coordinate with six short Ba−O contacts.[24] The relationship between the $CsRuO_4$ structure and that of scheelite was explored using the program AMPLIMODES, and we could not identify any structural relationship.[25] The structures are illustrated in Figure 2.

The differences between the various structures can be rationalized by considering the relative size of the cations; with the exception of $CsRuO_4$ the oxides have either the tetragonal scheelite or orthorhombic pseudoscheelite structure. That $RbRuO_4$, but not $RbOsO_4$, has the orthorhombic *Pnma* pseudoscheelite structure implies that the effective ionic radius of four-coordinate Ru^{VII} must be smaller than that of Os^{VII} since increasing r_A/r_B favors the orthorhombic structure.[5] Structures obtained by analysis of neutron diffraction data are available for the four potassium scheelites KBO_4 B = Tc, Os, Re, and Ru. Based on the unit cell volumes, 411.73(2), 409.753(2), 409.17(1), and 407.903(2) $Å^3$, respectively, and the *B*−O distances, 1.739(14), 1.732(2), 1.723(2), and 1.708(2) Å, it indeed appears that Ru^{VII} is the smallest of these cations. The *B*−O distance is sensitive to the size of the *A*-type cation. Except for *B* = Ru, the *B*−O distance decreases

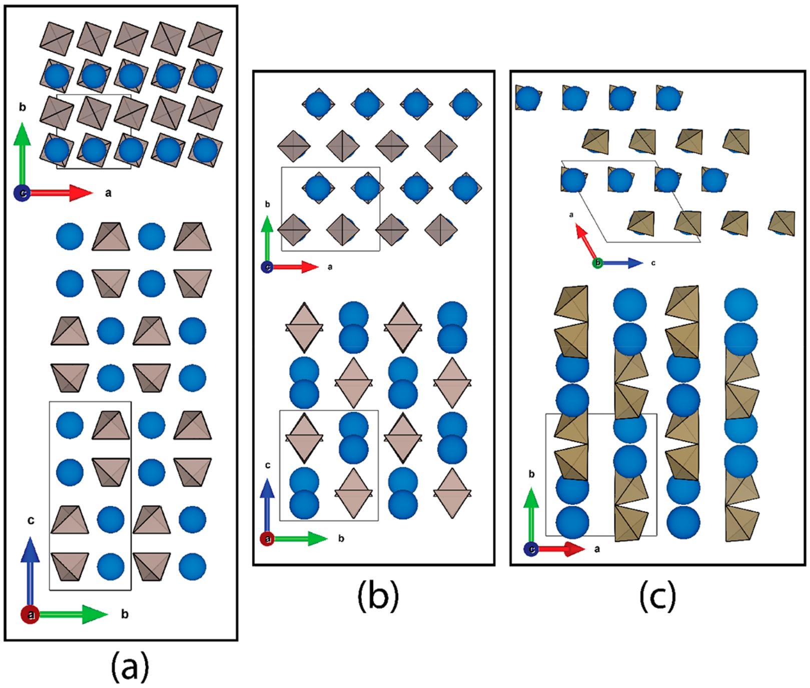

Figure 2. Representations of the crystal structures of $KRuO_4$ at room temperature, which adopts the scheelite structure in space group $I4_1/a$ (a), 2 × 2 unit cells are shown along the *c*-axis (top) and *a*-axis (bottom). A representation of the baryte-like structure of $CsRuO_4$ at room temperature in space group *Pnma* is shown in (b), similar to (a), 2 × 2 unit cells are shown along the *c*-axis (top) and *a*-axis bottom. A representation of the low temperature $P2_1/c$ structure of $CsOsO_4$ is shown in (c), 2 × 2 unit cells are shown projected along the *b*-axis (top) and *c*-axis (bottom). In all representations BO_4 tetrahedra are shown with omitted oxygen atoms at the vertices, and the *A* cation is indicated by blue spheres.

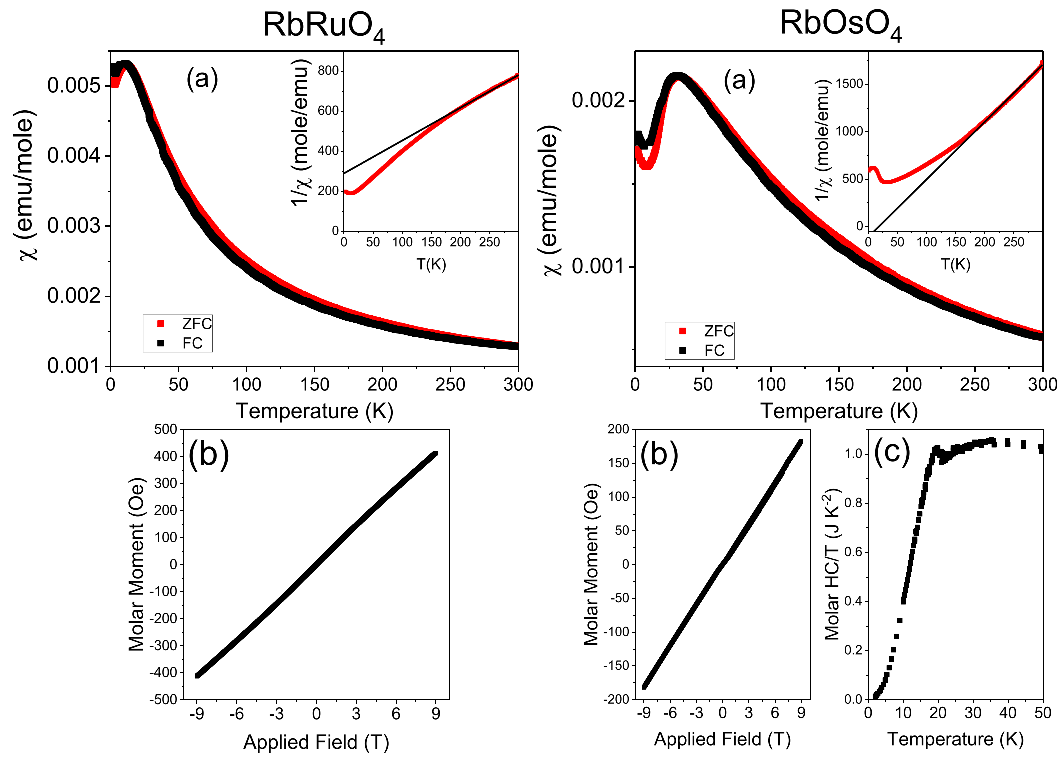

Figure 3. (a) Temperature dependence of the field cooled and zero field cooled magnetic susceptibilities (χ), (b) magnetization at 2 K, and (c) heat capacity for $RbRuO_4$ and $RbOsO_4$. The insets in (a) for both compounds are plots of the inverse susceptibility with the solid lines illustrating the fit of the high temperature data to the Curie−Weiss Law.

as the size of the *A*-type cation increases for the Tc, Os, and Re scheelites with Rb and Cs counterions. Based on our current work, we propose an effective ionic radius for four-coordinate Os^{VII} of 0.379 Å. This implies the effective bond valence parameters for four-coordinate Os^{VII} are R_0 = 1.92 and B = 0.37. An apparent outlier in this discussion is $CsRuO_4$ which

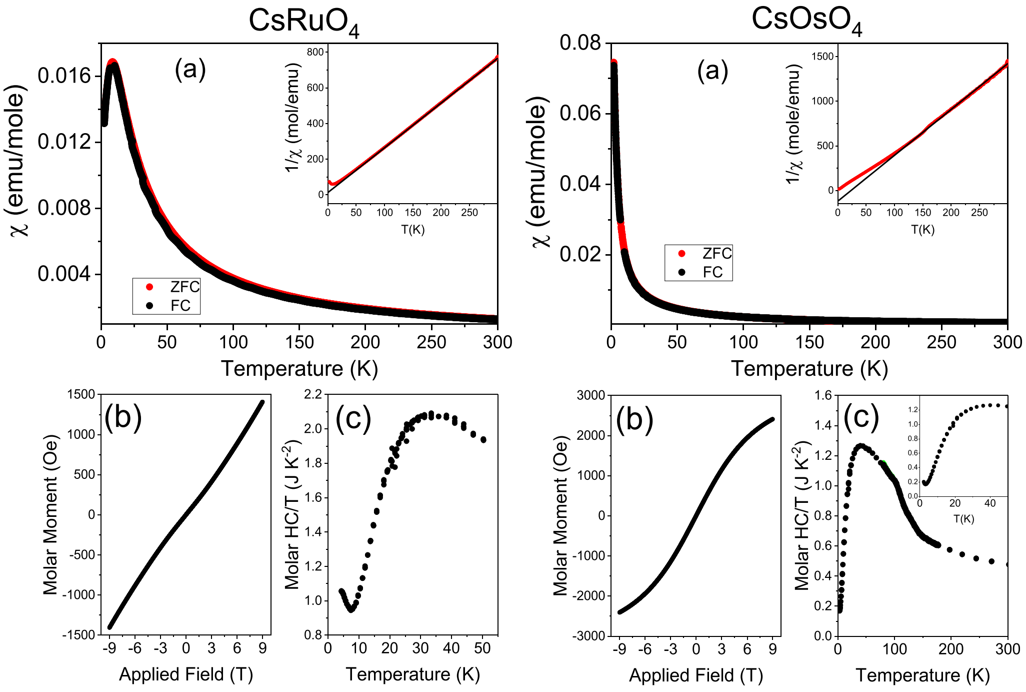

Figure 4. (a) Temperature dependence of the field cooled and zero field cooled magnetic susceptibilities (χ), (b) magnetization at 2 K, and (c) heat capacity for $CsRuO_4$ and $CsOsO_4$. The insets in (a) for both oxides are plots of the inverse susceptibility with the solid lines illustrating the fit of the high temperature data to the Curie−Weiss Law. The inset in (c) for $CsOsO_4$ highlights the minimum at low temperatures.

Table 2. Summary of the Magnetic Properties of the ABO_4 Oxides[a]

composition	$KRuO_4$	$RbRuO_4$	$CsRuO_4$	$KOsO_4$	$RbOsO_4$	$CsOsO_4$
T_N (K)	21		4	35	20	
$T_{\chi\max}$ (K)	37	12	9	61	32	
μ_{eff} (μ_B)	1.42	1.29	1.67	1.24	1.29	1.4
θ (K)	−43.8	−15.2	−6.9	−76.2	−35.8	−1.1
ΔS_{mag} (5.76 J K^{-1} mol^{-1})	1.35		1.64	1.39	1.38	

[a] T_N refers to the magnetic ordering temperature as determined from heat capacity data, and $T_{\chi\max}$ refers to the temperature corresponding to the maximum in magnetic susceptibility curves.

displays a baryte-type structure. The ABO_4 family of compounds encompasses a large number of structural types that contain tetrahedral BO_4 groups including scheelite, zircon, baryte, and fergusonite. A number of phenomenological rules for predicting structures have been employed to develop phase diagrams based on the size of the ions.[26−28] These suggest that the baryte structure will be favored over the scheelite structure as the size of the *B*-site cation is reduced, in keeping with our experimental studies.

2. Magnetic Susceptibility. Temperature dependent magnetic susceptibility and heat capacity measured between 300 and 2 K and isothermal magnetization measurements at 2 K are shown for the Rb and Cs compounds in Figures 3 and 4. The corresponding plots for the potassium salts are in the SI, Figure S4. For all samples except $CsOsO_4$, which remains paramagnetic to 2 K, a broad maximum and divergence of the ZFC and FC curves are apparent at low temperatures. Curie−Weiss fits, using data between 150 and 300 K, yielded effective magnetic moments of around 1.4 μ_B, see Table 2, which are reduced from the spin-only value of a simple d^1 system, 1.73 μ_B. In a tetrahedral field the d^1 ion will have an e^1t_2 electron configuration which gives a ^2E ligand field ground term in which the orbital contribution is expected to be quenched. Second order spin−orbit coupling will, however, reduce the moment. The small Jahn−Teller-type distortion of the BO_4 tetrahedra evident in the structural analysis, that will remove the degeneracy of the *e*-type states, is neglected here. That the observed moments of the three perruthenates are larger than the corresponding perosmates reflects the smaller spin−orbit coupling of 4*d* electrons compared to 5*d* electrons.

There is relatively good correlation between the Weiss constants (θ) and the Néel temperature (T_N) estimated from the heat capacity measurements, and this demonstrates the absence of magnetic frustration.[29] In all cases the frustration index $f = |\theta|/T_N$ is between 1 and 2, which is consistent with a lack of frustration. In general, the Néel temperatures estimated by plotting the Fisher heat capacity, $d(\chi T)/dT$ vs T, are in good agreement with the values estimated from the molar heat capacity plots.[30] For $CsRuO_4$ the Fisher heat capacity suggests the Néel temperatures to be near 6 K. That T_N is larger in $RbRuO_4$ than $T_{\chi\max}$ is puzzling; however, the variable temperature neutron diffraction data unequivocally demonstrates the presence of long-range antiferromagnetic ordering at low temperatures in $RbRuO_4$.

A feature in the heat capacity for $CsOsO_4$ is observed at approximately 150 K, and an anomaly is observed in the inverse susceptibility plots at about the same temperature, see Figure 4. The feature in the heat capacity was independent of

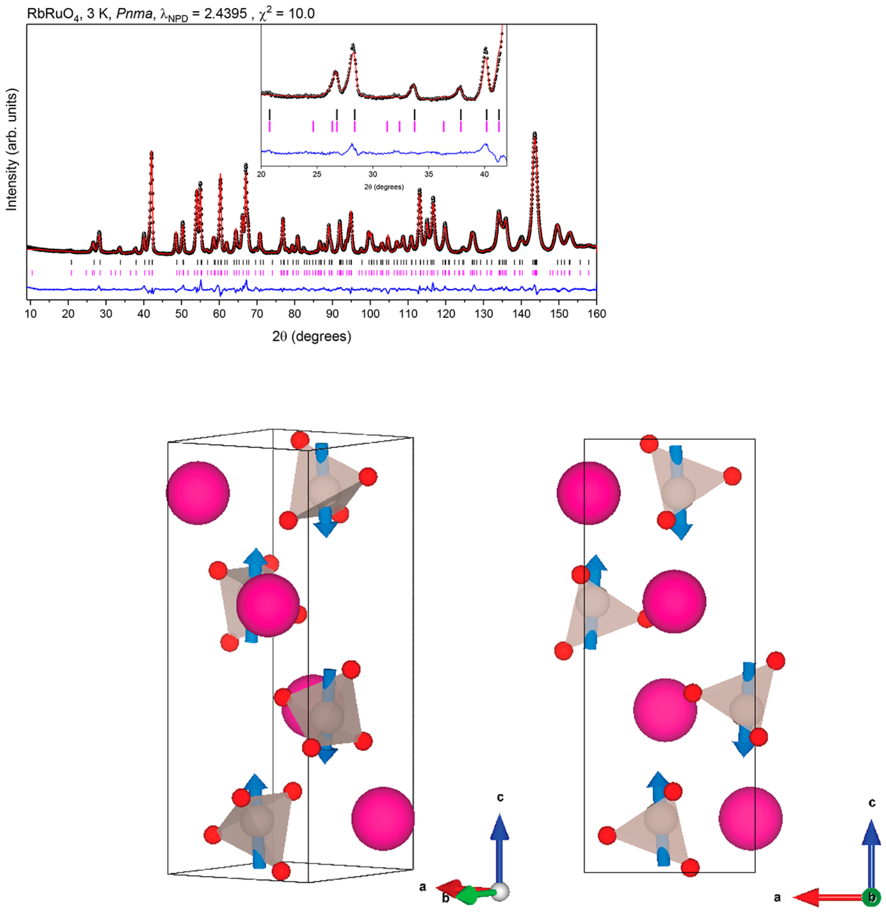

Figure 5. Results of the Rietveld refinement of neutron powder diffraction data for $RbRuO_4$ at 3 K. The black circles are the data, and the red line and blues lines are the calculated and difference profiles, respectively. The upper set of vertical tick marks is the allowed nuclear Bragg reflections, and the lower set is the allowed magnetic reflections. The k = (000) magnetic structure is also illustrated.

the applied magnetic field up to 5 T. This lack of magnetic field dependence indicates that it is due to a change in lattice enthalpy, that can be attributed to a crystallographic phase transition. The anomaly in the magnetic susceptibility is consistent with a slight change in the density of states of the Os cation, which accompanies a structural transition. Yamaura and Hiroi also observed a change in the heat capacity near 150 K and concluded that this was a result of a transition from the pseudoscheelite structure in space group *Pnma* to a monoclinic fergusonite-type structure in space group $I2/a$.[13] These workers, however, noted that they were unable to refine a structure in this space group. An alternate model in $P2_1/c$ is proposed below.

In all cases superexchange, which would involve the AO_8 polyhedra and entail a long *B*-O-*A*-O-*B* pathway, is expected to be very weak, rather direct exchange should be dominant. As suggested by Marjerrison et al.,[10] nearest neighbor interactions are expected to be the strongest, and this suggestion is apparently verified by noting how the increase in *B*−*B* separation correlates with the decrease in the Néel temperature in both the Ru and Os scheelites. $CsOsO_4$ is an outlier in this series reflecting the different configurations of the OsO_4 tetrahedra.

3. Magnetic Structures. Powder neutron diffraction data for the three oxides $KRuO_4$, $KOsO_4$, and $RbRuO_4$ measured at low temperatures showed that $KRuO_4$ and $KOsO_4$ retained the tetragonal $I4_1/a$ structure and that $RbRuO_4$ remained orthorhombic in *Pnma*. For both $KRuO_4$ and $KOsO_4$ a single very weak reflection that could be indexed as (110) appeared below the Néel temperature consistent with a magnetic structure with k = (000). As described in our earlier discussion of the magnetic structure of the $KOsO_4$ group theory analysis, performed with the ISODISTORT software suite, four possible irreducible representations namely Γ_1, Γ_3, Γ_5, and Γ_7 were indicated.[31,32] Of these only Γ_5 allows for intensity in the (110) but not the (002) reflection showing the magnetic structure to be antiferromagnetic with the moments parallel to the *c*-axis. For orthorhombic $RbRuO_4$ eight possible irreps were identified. Of these, Γ_{2+}, Γ_{3+}, and Γ_{4+} show ferromagnetic order and are therefore inconsistent with the magnetization data. The remaining representations show AFM ordering. For irreps Γ_{1+}, Γ_{2-}, and Γ_{3-} the moments are required to lie parallel to the *b*-axis. Irreps Γ_{1-} and Γ_{4+} show AFM ordering along the *c*-axis, with canting of moments within the 100 plane. All AFM irreps resulted in a similar quality of Rietveld fits to the NPD data, indicating that better data quality is required in order to unequivocally determine the magnetic structure of $RbRuO_4$. Nevertheless, a magnetic cell is tentatively proposed using Γ_{1-}, as this magnetic structure is effectively equal to that determined for $KRuO_4$ and $KOsO_4$, with a small AFM canting of magnetic moments within the 100 plane. A refinement profile using this model is shown in Figure 5. The magnetic moments were refined to be 0.77(24) μ_B along the *c* direction

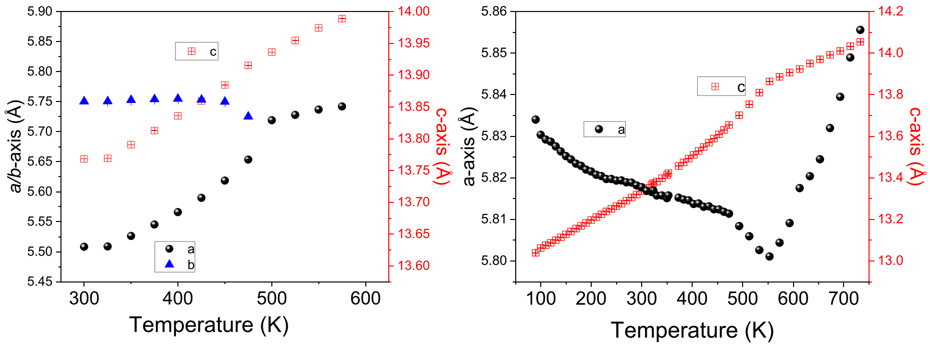

Figure 6. Temperature dependence of the lattice parameters for $RbRuO_4$ and $RbOsO_4$ determined from Rietveld refinements using S-XRD. $RbRuO_4$ exhibits a first order *Pnma*-$I4_1/a$ transition near 475 K, and $RbOsO_4$ shows a continuous $I4_1/a$ to $I4_1/amd$ transition near 550 K.

and 0.21(9) μ_B along the *a* direction. A representation of this magnetic structure is also shown in Figure 5.

The NPD profile of $RbOsO_4$ measured at 3 K using the Echidna diffractometer did not reveal any intensity at the (110) reflection; however, we note that the very weak moment of Os^{VII} $5d^1$ means that this reflection is expected to be extremely weak, and it appears that it is below the sensitivity of Echidna.[17] Likewise, it was not possible to observe a (110) reflection in the Echidna data for $KOsO_4$; this reflection, was, however, observed using the ToF diffractometer WISH.[12] This implies that the maximum ordered Os moment of $RbOsO_4$ is ~0.4 μ_B. Unfortunately, the $CsOsO_4$ sample showed evidence for decomposition, and we were unable to measure a satisfactory low temperature ND pattern for this. Studies of $CsRuO_4$ are ongoing.

4. Variable Temperature Structures. The structures of the six oxides were investigated using S-XRD from 90 K to high temperatures. $KOsO_4$ was found to remain tetragonal in space group $I4_1/a$ between 90 and 720 K, and there was no evidence for any thermally induced phase transitions. Scrutiny of Table 1 reveals that the atomic displacement parameters (ADPs) for the anions are invariably larger than that for the cations and that the ADPs are larger for the larger *A*-type cation than the smaller *B*-type cation. The anomalously large values for the oxygen in the refined structure of $RbOsO_4$ are believed to be a consequence of the proximity to the decomposition of the material. Despite the higher than typical values for the *A*-site cations, there is no reason to suspect that the atoms are displaced from the corresponding Wykoff sites.

Both $RbRuO_4$ and $RbOsO_4$ were found to undergo a structural phase transition upon heating. In the case of $RbRuO_4$, this was a *Pnma* to $I4_1/a$ transition near 475 K similar to that seen for $CsTcO_4$,[7] and the temperature dependence of the lattice parameters is illustrated in Figure 6. For $RbOsO_4$ a noticeable change in the anisotropic thermal expansion is seen at approximately 553 K, see Figure 6. The temperature dependence of the *c* parameter is very similar to what we described recently for $RbTcO_4$ and $RbReO_4$ where it was established that the change was due to a softening at the Γ point resulting in a $I4_1/amd$ to $I4_1/a$ phase transition.[7,22] These two structures differ in their orientation of the BO_4 tetrahedra; in $I4_1/a$ the tetrahedra are rotated about the *c*-axis, see Figure 7, and the *x* parameter for the oxygen in the general position 16*f* is a variable, whereas this is constrained to $x = 0$ for the equivalent 16*h* position in $I4_1/amd$. The cations are on special positions in both structures. The $I4_1/a$ to $I4_1/amd$ transition is allowed, by group theory, to be continuous, and the diffraction data is consistent with this. In the

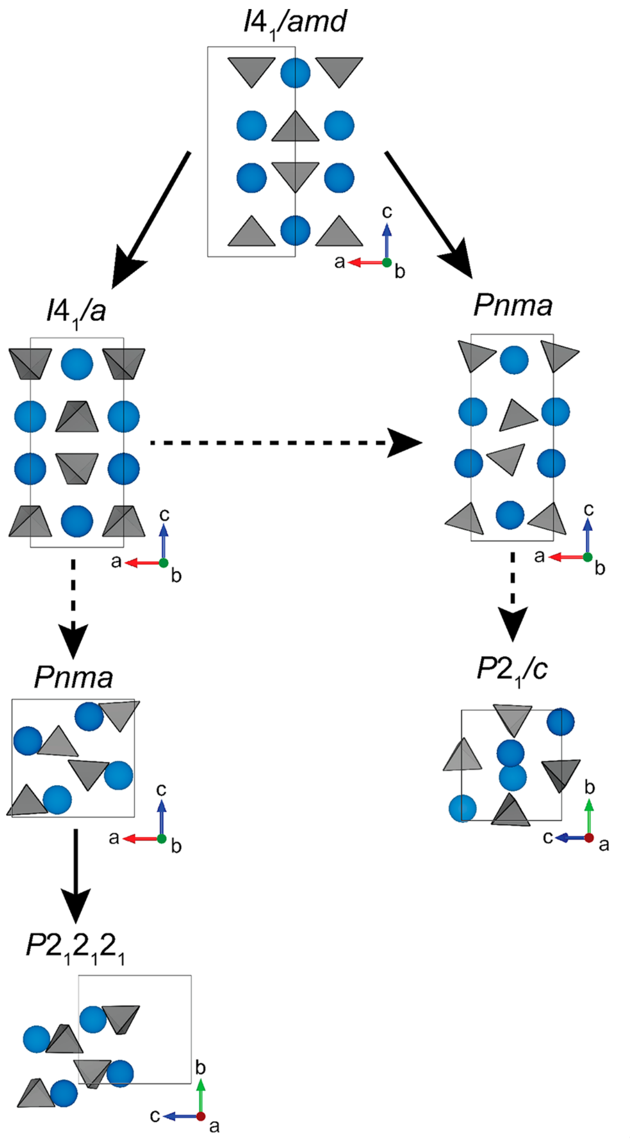

Figure 7. Representations of the ABO_4 structures identified in this work. In all cases the smaller *B*-type cation is at the center of the tetrahedra, and the larger *A*-type cation is represented by the spheres. The oxygen atoms are at the corners of the tetrahedra. The solid lines represent observed phase transitions that are allowed to be continuous, and the dashed lines observed transitions that must be first order.

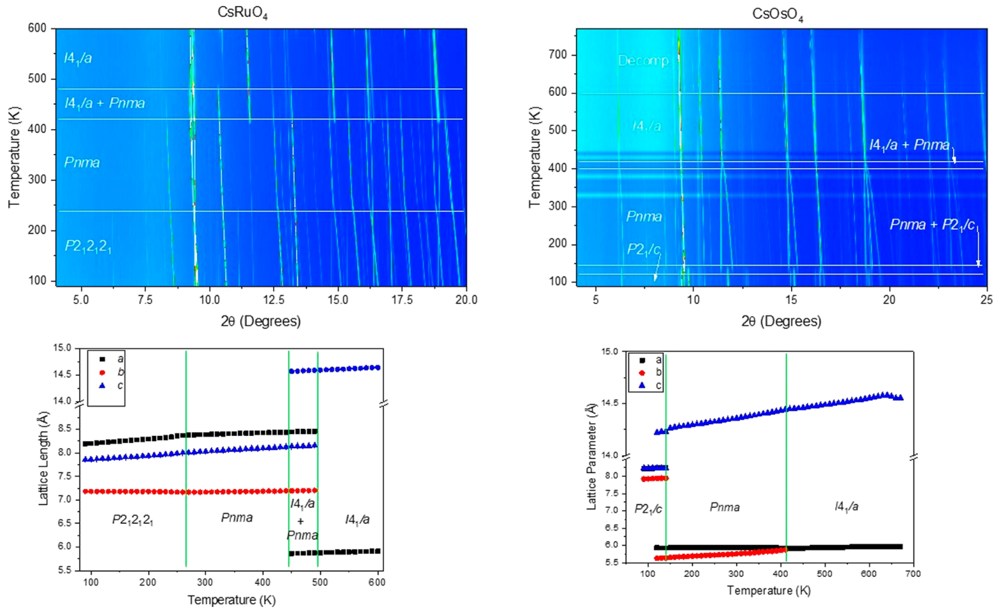

Figure 8. Portions of the S-XRD profiles and the temperature dependence of the lattice parameters for $CsRuO_4$ and $CsOsO_4$ determined from Rietveld refinements. $CsRuO_4$ exhibits a first order *Pnma*-$I4_1/a$ transition near 450 K and a continuous *Pnma*-$P2_12_12_1$ transition near 260 K, and $CsOsO_4$ shows two first order transitions from the *Pnma* structure to $I4_1/a$ near 400 K and to $P2_1/c$ near 110 K.

pseudoscheelite *Pnma* structure observed for $RbRuO_4$ the BO_4 tetrahedra are rotated in the *ab* plane, and this rotation is associated with softening at the *M*-point of the Brillouin zone. Group theory does not allow a continuous transition between these *Pnma* and $I4_1/a$ structures. It is possible that $RbRuO_4$ may realize the same $I4_1/amd$ structure as $RbOsO_4$ at higher temperatures; however, this could not be experimentally verified with the sample decomposing above 600 K. A number of ABO_4-type oxides undergo a pressure induced $I4_1/amd$ to $I4_1/a$ transition. However, as illustrated by the example of $YCrO_4$, invariably in these the low pressure phase has the $I4_1/amd$ zircon structure with $a \sim 7.089$ and $c \sim 6.281$ Å, while the high pressure phase has the $I4_1/a$ scheelite structure with $a \sim 5.0004$ and $c \sim 11.259$ Å.[33] In $YCrO_4$ the transition occurs near 3 GPa, and it is possible to recover the high pressure scheelite structure by quenching.[34] Thus, although increasing pressure can mimic the effect of decreasing temperature suggesting the $I4_1/a$ scheelite structure will be favored at high pressure or low temperatures, the reconstructive nature of the zircon to scheelite transition is clearly different than the continuous transition observed here for $RbOsO_4$.

A feature of Figure 6 is the weak negative thermal expansion (NTE) of the *a*-axis for $RbOsO_4$. A number of oxides that have been shown to display NTE including ZrW_2O_8,[35] ZrV_2O_7,[36] and Ag_2O,[37] and this is generally associated with low energy transverse motions of atoms that link together essentially rigid units.[38] The scheelite structure lacks obvious linear links, but there is evidence that transverse motions of more flexible linkers can facilitate NTE; and we postulate that the RbO_8 units that link the otherwise isolated BO_4 tetrahedra fulfill this role.[39]

Like $RbRuO_4$, $CsOsO_4$, which displays the distorted pseudoscheelite *Pnma* structure at room temperature, undergoes a first order phase transition to the undistorted $I4_1/a$ scheelite structure upon heating. The transition occurs at a slightly lower temperature than in $RbRuO_4$ with the orthorhombic and tetragonal phases coexisting over a limited temperature range ∼410−420 K, Figure 8. Above 420 K a single phase tetragonal scheelite structure is observed. Refinement profiles of the SXRD data at 410 K are shown in Figure S7, and both the *Pnma* and $I4_1/a$ structures are observed at this temperature. This behavior is very similar to that reported recently for $CsTcO_4$ and $CsReO_4$.[7,22] $CsOsO_4$ rapidly decomposed above 600 K. The decomposition of this, and of the other Ru and Os oxides studied here, at high temperatures contrasts that seen for the $ATcO_4$ and $AReO_4$ compounds, where the room temperature structures can be recovered from the high temperature melts upon cooling.[7]

As anticipated from the heat capacity measurements, $CsOsO_4$ undergoes a second phase transition upon cooling, see Figure 8. We initially tested the $I2/a$ fergusonite-type model, suggested by Yamaura and Hiroi;[13] however, it was immediately realized that this was wrong. The S-XRD profile measured at 90 K could be indexed to a primitive monoclinic structure with $a = 8.2228$, $b = 7.921734$, $c = 8.2303$ Å, and $\beta = 119.085(6)°$, and this was identified as being in space group $P2_1/c$. The structure was then solved using charge flipping and refined. The lattice parameters are inconsistent with a scheelite related structure but are similar to the parameters of the orthorhombic baryte-type $CsRuO_4$ structure ($a = 8.40128(1)$, $b = 7.17776(1)$, $c = 8.04343(1)$ Å). Scrutiny of the diffraction data showed evidence of the coexistence of the high temperature *Pnma* and low temperature $P2_1/c$ phases between 140 and 120 K, indicating that the transition between these two structures is first order. A refinement profile of S-XRD data collected at 90 K for $CsOsO_4$ is shown in Figure S6. An increase in heat capacity is also observed at approximately 3 K, shown in the inset of Figure 4c. Although there is insufficient data in this temperature region to characterize this feature, it may indicate long-range magnetic order, and future characterization is required.

The situation for $CsRuO_4$ is more complex. As stated above, at room temperature $CsRuO_4$ is found in the orthorhombic baryte-type structure. Heating results in a first order transition to the tetragonal scheelite structure near 420 K. Cooling below 270 K results in the appearance of additional reflections in S-

XRD data, and the cell could be indexed to a second orthorhombic space group $P2_12_12_1$. Representative Rietveld profiles are shown in Figure S6. This structure consists of chains of edge sharing CsO_{10} and RuO_4 polyhedra. This low temperature structure was confirmed by single crystal XRD data collected at 90 K. $BaSO_4$ itself has been reported to undergo a $Pnma \rightarrow P2_12_12_1$ transition at high pressures around 27 GPa.[40] The same transition has been observed at high pressure in $PbSO_4$.[41] The high pressure or postbaryte phase is described in space group $P2_12_12_1$ (No. 19) which is a subgroup of the *Pnma* (No. 62) space group of the initial baryte-type structure. Whereas this transition has been described as first order for both $BaSO_4$ and $PbSO_4$, in the present case the transition is clearly continuous.[40,41] The two structures differ in the orientation of the RuO_4 tetrahedra (see Figure 2), and the transformation between them can be described by Γ_{1-}. The high magnetic entropy determined from heat capacity for this compound suggests strong magnetic interactions for this structure.

As described above, the three scheelite related structures in space groups $I4_1/amd$, $I4_1/a$, and *Pnma* differ in their orientation of the BO_4 tetrahedra. The diffraction data are consistent with the conclusions from group theory that the transition between the two tetragonal structures, $I4_1/amd$ and $I4_1/a$, as seen in the two Rb containing oxides is continuous, whereas the structure between the tetragonal $I4_1/a$ and orthorhombic *Pnma* structures seen in $CsOsO_4$ is first order. The formation of a second structural type that we describe as a distorted baryte-type is surprising but is consistent with Bastide's analysis of ABO_4-type structures.[26] Despite both $CsRuO_4$ and $CsOsO_4$ being found in the same space group, there is no relationship between the structures, and the transformation between the distorted baryte and scheelite as observed in $CsRuO_4$ is first order.

CONCLUDING REMARKS

Crystal structures of six ABO_4 oxides (A = K, Rb, or Cs; B = Ru or Os) at room temperature have been determined using a combination of powder neutron and synchrotron X-ray diffraction, and their magnetic properties were established. Except for $CsRuO_4$, all the samples exhibit either a tetragonal scheelite or orthorhombic pseudoscheelite structure at room temperature, with the symmetry lowering resulting from a decrease in the ratio of the ionic radii r_A/r_B. Comparing the structures of $KRuO_4$ and $KOsO_4$ provides the first direct experimental evidence for the small increase in the ionic radius of four-coordinate Os^{VII} over that of Ru^{VII}. $RbRuO_4$ undergoes a first order $Pnma$-$I4_1/a$ transition upon heating as is also observed in $CsOsO_4$. Group theory does not allow a continuous $Pnma$-$I4_1/a$ transition for these oxides reflecting the different orientation of the BO_4 tetrahedra. $RbOsO_4$ displays anomalous thermal expansion behavior associated with a continuous $I4_1/a$ to $I4_1/amd$ transition as seen recently in both $RbTcO_4$ and $RbReO_4$.[12,22] While the high temperature phase transition behavior seen for $CsOsO_4$ is similar to that observed in the isostructural Tc and Re oxides, the first order transition observed upon cooling has no analogy in these oxides, rather it involves a reconstructive transition to a new $P2_1/c$ polymorph rather than the $I2/a$ fergusonite structure observed in oxides such as $LaNbO_4$.[42] At room temperature $CsRuO_4$ has a structure that is more closely related to baryte ($BaSO_4$) than scheelite. This undergoes a continuous transition to a postbaryte-type structure upon cooling, analogous to the high pressure behavior displayed by other ABO_4 oxides including $PbSO_4$.[41] Interestingly, heating $CsRuO_4$ induces a reconstructive first order transition to the tetragonal scheelite structure observed in the other Ru and Os oxides described here. Errandonea and co-workers have reported pressure dependent structural studies for a number of ABO_4-type oxides but no examples with Ru or Os, and a reoccurring feature of this work is the susceptibility of these materials to undergo reconstructive phase transitions.[33] While resulting in considerable structural diversity, the preponderance of first order phase transitions in the ABO_4 oxides makes elucidation of the systematics controlling the formation of particular structural motifs challenging and suggests the diagram of Bastide needs revision.[26]

The oxides display long-range antiferromagnetic ordering of the $S = 1/2$ spins at low temperatures with the Néel temperature of the Os oxides generally being higher, reflecting the more diffuse nature of the 5*d* vs 4*d* orbitals. Direct, rather than superexchange, exchange appears to be dominant with an increase in the metal−metal separation resulting in a decrease in the Néel temperature in both the Ru and Os scheelites. $CsOsO_4$ is an outlier in this series reflecting the different configurations of the OsO_4 tetrahedra. The high magnetic entropy determined from heat capacity for $CsRuO_4$ suggests strong magnetic interactions for this structure. Low temperature neutron diffraction measurements would prove valuable in determination of the magnetic structure of this compound.

ASSOCIATED CONTENT

Supporting Information

The Supporting Information is available free of charge at https://pubs.acs.org/doi/10.1021/acs.inorgchem.9b03118.

Rietveld profiles of the S-XRD and NPD fits for $KOsO_4$, $KRuO_4$ and $CsOsO_4$ at room temperature, representations of refined structures, magnetic susceptibility and heat capacity curves for $KRuO_4$ and $KOsO_4$, variable temperature S-XRD profiles of $CsRuO_4$ and $CsOsO_4$, and single crystal X-ray structural details (PDF)

Accession Codes

CCDC 1964054−1964062 contain the supplementary crystallographic data for this paper. These data can be obtained free of charge via www.ccdc.cam.ac.uk/data_request/cif, or by emailing data_request@ccdc.cam.ac.uk, or by contacting The Cambridge Crystallographic Data Centre, 12 Union Road, Cambridge CB2 1EZ, UK; fax: +44 1223 336033.

AUTHOR INFORMATION

Corresponding Author

Brendan J. Kennedy − *School of Chemistry, The University of Sydney, Sydney 2006, Australia;* orcid.org/0000-0002-7187-4579; Email: Brendan.Kennedy@Sydney.edu.au

Authors

Sean Injac − *School of Chemistry, The University of Sydney, Sydney 2006, Australia*

Alexander K. L. Yuen − *School of Chemistry, The University of Sydney, Sydney 2006, Australia*

Maxim Avdeev − *School of Chemistry, The University of Sydney, Sydney 2006, Australia; Australian Centre for Neutron Scattering, Australian Nuclear Science and Technology Organisation, ANSTO, , Lucas Heights 2234, Australia;* orcid.org/0000-0003-2366-5809

Chun-Hai Wang − *School of Chemistry, The University of Sydney, Sydney 2006, Australia*
Peter Turner − *School of Chemistry, The University of Sydney, Sydney 2006, Australia*
Helen E. A. Brand − *Australian Synchrotron, Australian Nuclear Science and Technology Organisation, ANSTO, , Clayton 3168, Australia*

Complete contact information is available at:
https://pubs.acs.org/10.1021/acs.inorgchem.9b03118

Notes

The authors declare no competing financial interest.

■ ACKNOWLEDGMENTS

B.J.K. acknowledges the support of the Australian Research Council for this work that was, in part, performed at the powder diffraction beamline at the Australian Synchrotron and at the Australian Centre for Neutron Scattering. This research was facilitated by access to Sydney Analytical, a core research facility at the University of Sydney

■ REFERENCES

(1) Forte, F.; Guerra, D.; Autieri, C.; Romano, A.; Noce, C.; Avella, A. Strong spin-orbit effects in transition metal oxides with tetrahedral coordination. *Phys. B* **2018**, *537*, 184−187.

(2) Zhao, Q.; Sim, J. H.; Zhang, Z.; Su, H.; Han, F.; Zhang, Q.; Tian, B.; Xu, Q.; Han, M. J.; Duan, C. G.; Mitchell, J. F. Tetrahedral coordination and low-spin configuration in a 5d oxide. *Physical Review Materials* **2019**, *3* (6), 063607.

(3) Range, K. J.; Rogner, P.; Heyns, A. M.; Prinsloo, L. C. An X-ray, Raman and IR study of α-CsReO$_4$, the high-temperature modification of cesium perrhenate. *Z. Naturforsch., B: J. Chem. Sci.* **1992**, *47* (11), 1513−1520.

(4) Rogner, P.; Range, K. J. The crystal-structure of β-thallium perrhenate. *Z. Anorg. Allg. Chem.* **1993**, *619* (6), 1017−1022.

(5) Rogner, P.; Range, K. J. The crystal-structure of β-CsReO$_4$, the room-temperature modification of cesium perrhenate. *Z. Naturforsch., B: J. Chem. Sci.* **1993**, *48* (5), 685−687.

(6) Rogner, P.; Range, K. J. Structure refinement of rubidium perrhenate at 297 and 159 K. *Z. Naturforsch., B: J. Chem. Sci.* **1993**, *48* (2), 233−234.

(7) Kennedy, B. J.; Injac, S.; Thorogood, G. J.; Brand, H. E. A.; Poineau, F. Structures and Phase Transitions in Pertechnetates. *Inorg. Chem.* **2019**, *58* (15), 10119−10128.

(8) Weaver, J.; Soderquist, C. Z.; Washton, N. M.; Lipton, A. S.; Gassman, P. L.; Lukens, W. W.; Kruger, A. A.; Wall, N. A.; McCloy, J. S. Chemical Trends in Solid Alkali Pertechnetates. *Inorg. Chem.* **2017**, *56* (5), 2533−2544.

(9) Silverman, M. D.; Levy, H. A. Crystal structure of potassium perruthenate, KRuO$_4$. *J. Am. Chem. Soc.* **1954**, *76* (12), 3317−3319.

(10) Marjerrison, C. A.; Mauws, C.; Sharrna, A. Z.; Wiebe, C. R.; Derakhshan, S.; Boyer, C.; Gaulin, B. D.; Greedan, J. E. Structure and Magnetic Properties of KRuO$_4$. *Inorg. Chem.* **2016**, *55* (24), 12897−12903.

(11) Levason, W.; Tajik, M.; Webster, M. Synthesis and properties of alkali-metal tetraoxo-osmate(VII) compounds. *J. Chem. Soc., Dalton Trans.* **1985**, No. 8, 1735−1736.

(12) Injac, S.; Yuen, A. K. L.; Avdeev, M.; Orlandi, F.; Kennedy, B. J. Structural and magnetic studies of KOsO$_4$, a 5d^1 quantum magnet oxide. *Phys. Chem. Chem. Phys.* **2019**, *21* (14), 7261−7264.

(13) Yamaura, J.-i.; Hiroi, Z. Crystal structure and magnetic properties of the 5d transition metal oxides AOsO$_4$ (A = K, Rb, Cs). *Phys. Rev. B: Condens. Matter Mater. Phys.* **2019**, *99* (15), 155113.

(14) Song, Y. J.; Ahn, K. H.; Lee, K. W.; Pickett, W. E. Unquenched e$_g$^{1} orbital moment in the Mott-insulating antiferromagnet KOsO$_4$. *Phys. Rev. B: Condens. Matter Mater. Phys.* **2014**, *90* (24), 245117.

(15) Hayami, S.; Kusunose, H.; Motome, Y. Emergent odd-parity multipoles and magnetoelectric effects on a diamond structure: Implication for the 5d transition metal oxides AOsO$_4$ (A = K, Rb, and Cs). *Phys. Rev. B: Condens. Matter Mater. Phys.* **2018**, *97* (2), 024414.

(16) Djerassi, C.; Engle, R. R. Oxidations with ruthenium tetroxide. *J. Am. Chem. Soc.* **1953**, *75* (15), 3838−3840.

(17) Avdeev, M.; Hester, J. R. ECHIDNA: a decade of high-resolution neutron powder diffraction at OPAL. *J. Appl. Crystallogr.* **2018**, *51*, 1597−1604.

(18) Wallwork, K. S.; Kennedy, B. J.; Wang, D. The high resolution powder diffraction beamline for the Australian Synchrotron. *AIP Conf Proc.* **2006**, *879*, 879−882.

(19) Rodriguez-Carvajal, J. Recent advances in magnetic-structure determination by neutron powder diffraction. *Phys. B* **1993**, *192* (1−2), 55−69.

(20) Roisnel, T.; Rodriguez-Carvajal, J. WinPLOTR: A Windows tool for powder diffraction pattern analysis. In *Epdic 7: European Powder Diffraction, Pts 1 and 2*; Delhez, R., Mittemeijer, E. J., Eds.; 2001; Vol. 378−381, pp 118−123, DOI: 10.4028/www.scientific.net/MSF.378-381.118.

(21) Shannon, R. D. Revised effective ionic-radii and systematic studies of interatomic distances in halides and chalcogenides. *Acta Crystallogr., Sect. A: Cryst. Phys., Diffr., Theor. Gen. Crystallogr.* **1976**, *32* (SEP1), 751−767.

(22) Chay, C.; Avdeev, M.; Brand, H. E. A.; Injac, S.; Whittle, T. A.; Kennedy, B. J. Crystal Structure and Phase Transition Behaviour in the 5d transition metal oxides AReO$_4$ (A = K, Rb, Cs and Tl). *Dalton Transactions* **2019**, *48*, 17524−17532.

(23) Santamaria-Perez, D.; Chulia-Jordan, R.; Daisenberger, D.; Rodriguez-Hernandez, P.; Munoz, A. Dense Post-Barite-type Polymorph of PbSO$_4$ Anglesite at High Pressures. *Inorg. Chem.* **2019**, *58* (4), 2708−2716.

(24) Colville, A. A.; Staudhammer, K. A Refinement of the Structure of Barite. *Am. Mineral.* **1967**, *52* (11−12), 1877−1880.

(25) Perez-Mato, J. M.; Orobengoa, D.; Aroyo, M. I. Mode crystallography of distorted structures. *Acta Crystallogr., Sect. A: Found. Crystallogr.* **2010**, *66* (5), 558−590.

(26) Bastide, J. P. Simplified systematics of the compounds ABX$_4$ (X= O^{2-},F-) and possible evolution of their crystal-structures under pressure. *J. Solid State Chem.* **1987**, *71* (1), 115−120.

(27) Clavier, N.; Podor, R.; Dacheux, N. Crystal chemistry of the monazite structure. *J. Eur. Ceram. Soc.* **2011**, *31* (6), 941−976.

(28) Crichton, W. A.; Parise, J. B.; Antao, S. M.; Grzechnik, A. Evidence for monazite-, Barite-, and AgMnO$_4$ (distorted Barite)-type structures of CaSO$_4$ at high pressure and temperature. *Am. Mineral.* **2005**, *90* (1), 22−27.

(29) Greedan, J. E. Geometrically frustrated magnetic materials. *J. Mater. Chem.* **2001**, *11* (1), 37−53.

(30) Fisher, M. E. Relation between specific heat and susceptibility of an antiferromagnet. *Philos. Mag.* **1962**, *7* (82), 1731−1743.

(31) Campbell, B. J.; Stokes, H. T.; Tanner, D. E.; Hatch, D. M. ISODISPLACE: a web-based tool for exploring structural distortions. *J. Appl. Crystallogr.* **2006**, *39*, 607−614.

(32) Stokes, H. T.; Hatch, D. M.; Campbell, B. J. *ISODISTORT, ISOTROPY Software Suite*. iso.byu.edu (accessed Jan 23, 2020).

(33) Errandonea, D.; Kumar, R.; Lopez-Solano, J.; Rodriguez-Hernandez, P.; Munoz, A.; Rabie, M. G.; Puche, R. S. Experimental and theoretical study of structural properties and phase transitions in YAsO$_4$ and YCrO$_4$. *Phys. Rev. B: Condens. Matter Mater. Phys.* **2011**, *83* (13), 134109.

(34) Long, Y. W.; Yang, L. X.; Yu, Y.; Li, F. Y.; Yu, R. C.; Jin, C. Q. Synthesis, structure, magnetism and specific heat of YCrO$_4$ and its zircon-to-scheelite phase transition. *Phys. Rev. B: Condens. Matter Mater. Phys.* **2007**, *75* (10), 104402.

(35) Tucker, M. G.; Goodwin, A. L.; Dove, M. T.; Keen, D. A.; Wells, S. A.; Evans, J. S. O. Negative thermal expansion in ZrW$_2$O$_8$: Mechanisms, rigid unit modes, and neutron total scattering. *Phys. Rev. Lett.* **2005**, *95* (25), 255501.

(36) Yamamura, Y.; Horikoshi, A.; Yasuzuka, S.; Saitoh, H.; Saito, K. Negative thermal expansion emerging upon structural phase transition in ZrV_2O_7 and HfV_2O_7. *Dalton Transactions* **2011**, *40* (10), 2242−2248.

(37) Kennedy, B. J.; Kubota, Y.; Kato, K. Negative thermal expansion and phase transition behaviour in Ag_2O. *Solid State Commun.* **2005**, *136* (3), 177−180.

(38) Miller, W.; Smith, C. W.; Mackenzie, D. S.; Evans, K. E. Negative thermal expansion: a review. *J. Mater. Sci.* **2009**, *44* (20), 5441−5451.

(39) Sapnik, A. F.; Geddes, H. S.; Reynolds, E. M.; Yeung, H. H. M.; Goodwin, A. L. Compositional inhomogeneity and tuneable thermal expansion in mixed-metal ZIF-8 analogues. *Chem. Commun.* **2018**, *54* (69), 9651−9654.

(40) Santamaría-Pérez, D.; Chuliá-Jordán, R. Compression of mineral Barite, $BaSO_4$: a structural study. *High Pressure Res.* **2012**, *32* (1), 81−88.

(41) Santamaria-Perez, D.; Chulia-Jordan, R.; Daisenberger, D.; Rodriguez-Hernandez, P.; Muñoz, A. Dense Post-Barite-type Polymorph of $PbSO_4$ Anglesite at High Pressures. *Inorg. Chem.* **2019**, *58* (4), 2708−2716.

(42) Arulnesan, S. W.; Kayser, P.; Kimpton, J. A.; Kennedy, B. J. Studies of the fergusonite to scheelite phase transition in $LnNbO_4$ orthoniobates. *J. Solid State Chem.* **2019**, *277*, 229−239.